Environmental Science & Technology

pubs.acs.org/est

Article

Summertime Clean-Background Ozone Concentrations Derived from Ozone Precursor Relationships are Lower than Previous Estimates in the Southeast United States

Qiyang Yan, Yuhang Wang,* Ye Cheng, and Jianfeng Li

Cite This: *Environ. Sci. Technol.* 2021, 55, 12852−12861

Read Online

ACCESS | Metrics & More | Article Recommendations | Supporting Information

ABSTRACT: Background ozone in this study is defined as the amount of ozone that is not affected by the emissions of ozone precursors in the region of study and is transported from the distant troposphere or the stratosphere. It is one of the factors that must be considered in regional ozone control strategies. Different methods have been applied to define the background ozone level. We develop a new method based on the O_3−CO−HCHO relationships, which can be applied to both observation and modeling data for regions with high isoprene emission ozone, such as the Southeast United States. We make use of the extensive aircraft and surface observations in the Southeast in the summer of 2013. Compared to the diagnostic results using the relationship of O_3−NO_z (total reactive nitrogen excluding nitrogen oxides), zero-emission (model-only), and 5th percentile methods, the new method is most consistent using observation or model data and the resulting background ozone concentrations are 4−50% lower than the other methods for field campaigns. Using this method, we find that the summertime background ozone at the surface is in the range of 10−15 ppbv in the inland areas of the Southeast, which is lower than that reported in previous studies. This background ozone tends to increase from urban centers to rural regions and from the surface to higher altitude due to changing ozone lifetime driven by anthropogenic emissions and dry deposition to the surface. The better quantification of background ozone using the new method highlights the importance of the contributions by natural emissions to ozone and the necessity to control anthropogenic emissions in ozone nonattainment areas of the Southeast.

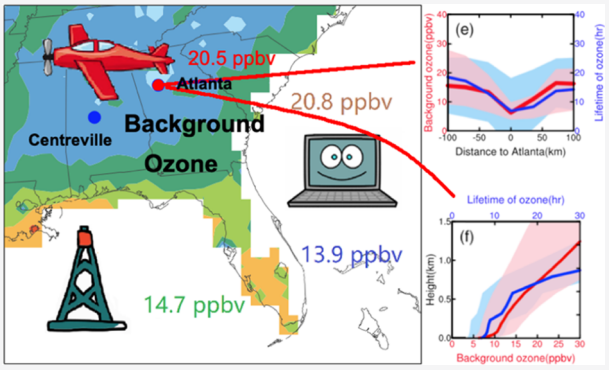

KEYWORDS: *background ozone, ozone precursor relationships, nonattainment, air pollution, SOAS and SENEX*

1. INTRODUCTION

"Surface-level" ozone is regulated by the National Ambient Air Quality Standards (NAAQS) in the United States.[1] Summer is the season of high ozone concentrations in polluted regions, although the ozone season can expand beyond summer as a result of climate change.[2] In the past several decades, the Clean Air Act Amendments and their enforcement have led to large reductions of anthropogenic emissions of nitrogen oxides (NO_x = NO + NO_2) and volatile organic compounds (VOC). However, summertime ozone concentrations over large regions of the western United States (excluding California) have insignificant and even a small increasing trend in contrast to significant decreases over the eastern United States and California.[3−5] One potential contributor is an increase of background ozone concentrations in the West.[5] However, some of the uncertainties in defining the regional ozone background were extensively discussed in the earlier works by Fiore et al.[6,7] and were subsequently analyzed.[8−13] The recent assessments by Jaffe et al.[14] again emphasized the significant contributions and large uncertainties of background ozone.

There are many approaches to reduce the uncertainties of model-simulated background ozone, including modeling process-level intercomparison exercises and improving emissions, physical and chemical processes in the model. Ultimately, however, observation-based background ozone estimates will be needed as the ground truth. We note that the analyses of remote and background ozone sites[15,16] are for what Cooper et al.[17] termed "baseline" ozone, which includes ozone produced from North American emissions. The "baseline" ozone, therefore, is higher than the background ozone. Other attempts to estimate background ozone have been made using the relationships between ozone and its

Received: May 10, 2021
Revised: July 31, 2021
Accepted: September 7, 2021
Published: September 21, 2021

https://doi.org/10.1021/acs.est.1c03035
Environ. Sci. Technol. 2021, 55, 12852−12861

precursors. Given the important role of NO_x in ozone photochemical production and the previously found dependence of ozone on NO_x and NO_y to derive ozone production efficiency values,[18,19] it is not surprising that the relationships of ozone with NO_z [defined as total reactive nitrogen (NO_y)−NO_x ($NO + NO_2$)] were explored to define background ozone[15,20] by extrapolating the O_3−NO_z linear regression line to the zero-value point of NO_z, the corresponding ozone value presumably represents a background value (hereafter referred to as the O_3−NO_z method).

Background ozone is not a well-defined term.[14] If a location is downwind from a polluted urban region, transported high ozone concentrations can be considered as a background or "baseline" ozone level for the site.[6,21] Using the type of operational definition, background ozone concentrations would vary depending on the applications and are therefore difficult to compare among different studies. For example, if we extend from one site to a region, the influence from the upwind city emissions would vary with time and location in the region. In this case, defining a clean background not affected by the emissions from the upwind city is more objective and more easily intercomparable than trying to incorporate the effect of the city emissions in the background ozone calculation. In this work, we define a clean-background ozone as the portion of ozone that does not have chemical signatures, showing ozone production from anthropogenic or natural emissions of ozone precursors. This definition is akin to deriving the ozone background using the O_3−NO_z regression method,[15] but it is more refined. Hereafter, we refer to this clean-background ozone level as the ozone background in this work.

Another well-known linear relationship is between ozone and its precursor, CO.[22−31] Cheng et al.[32] examined the measurements from the DISCOVER-AQ campaign in July 2011 over the Baltimore−Washington area and found that the O_3−CO correlation does not vary significantly with time or altitude in the boundary layer and the observations are simulated well by our Regional chEmistry and trAnsport Model (REAM). Their analysis suggests that due to the decrease of anthropogenic primary CO emissions during the past decades, the contribution from biogenic isoprene oxidation to the observed O_3−CO regression slope is as large as primary anthropogenic CO emissions in contrast to the finding that anthropogenic emissions are the main contributors to the observed O_3−CO relationship in the 1980s and early 1990s.[22]

Cheng et al.[33] went a step further and examined the utility of the robust linear regression relationships of observed O_3−HCHO, O_3−CO, and CO−HCHO, which do not vary significantly with time (11 A.M. to 4 P.M.) or altitude in the boundary layer during the DISCOVER-AQ 2011 experiment. They found that these relationships can be used to provide a fast-response estimator of surface ozone when the concentrations of CO and HCHO are known in the Southeast. What we will explore in this study is how the relationships of ozone with CO and HCHO can be applied to compute a clean background ozone (hereafter referred to as the O_3−CO−HCHO method) such that the background ozone is separated into two components: (1) a zero-chemical-signature using the O_3−CO−HCHO method and (2) a regional background ozone that still has chemical signatures associated with ozone-precursor relationships.

In this study, we applied the methods of O_3−CO−HCHO,[33] O_3−NO_z,[15,20] and 5th percentile ozone[34] to surface and aircraft observations during the Southern Oxidant and Aerosol Study (SOAS) and Southeast Nexus (SENEX) campaigns in the summer of 2013 in the Southeast and the corresponding 3-D model simulation results. A model-only zero-emission method[7,13] was also used. The background ozone concentrations derived from the observations and model results using various methods are compared to investigate the potential biases of the methods. We will show the distribution of summertime background ozone based on model simulations and discuss the implications for air quality management.

2. METHODS AND DATA SETS

2.1. Observation Data Sets. We made use of the extensive observations during the Southeast Atmosphere Study (SAS) from 1 June 2013 to 15 July 2013.[35] The SAS includes two field campaigns: SOAS and SENEX.[36] SOAS provides detailed ground measurements of O_3, NO_x, NO_y, CO, and HCHO at the SouthEastern Aerosol Research and Characterization Network (SEARCH) site—Centreville, Alabama from 1 June to 15 July. It is a typical rural site in the Southeast surrounded by mixed forest where biogenic emissions are dominant.[37] Along with SOAS, the National Oceanic and Atmospheric Administration (NOAA) WP-3D aircraft was deployed during the SENEX campaign to extensively measure O_3, NO_x, NO_y, CO, and HCHO concentrations around Smyrna, Tennessee.[38] During the SENEX campaign, a total of 12 daytime flights were conducted to make atmospheric measurements in the lower troposphere. In this study, we selected the SENEX measurements in the Southeast (domain shows in Figure 3) at 0−1 km to derive the background ozone concentrations in the boundary layer in order to ensure the robustness of our O_3−CO−HCHO analysis results in the region where biogenic emissions dominate VOC reactivity and compared them to the ozone background derived from the SOAS surface data. For consistency, NO_y measurements using the chemiluminescence instruments were used to compute observed NO_z concentrations for both campaigns. Table S1 summarizes the instruments and uncertainties for O_3, NO_x, NO_y, CO, and HCHO measurements.[39−43]

2.2. 3-D REAM Model. We applied the REAM in this study to compute the regional background ozone in the Southeast during the SAS. REAM is a 3-D regional model which has been evaluated in a number of tropospheric chemistry and transport studies in the United States and China.[2,44−53] The model domain of REAM is shown in Figure S5, with 30 vertical layers in the troposphere, and the horizontal resolution is 36 × 36 km^2. Simulations used in this study utilized lateral boundary conditions taken from a 2° × 2.5° GEOS-Chem model (v11.01) simulation.[54] Henderson et al.[55] evaluated the GEOS-Chem model with respect to its ability to provide lateral boundary conditions of ozone and its precursors for the contiguous United States (CONUS) domain to regional models and showed good performance in the summer. The model is driven by assimilated meteorological fields from a weather research and forecasting (WRF) simulation constrained by the Climate Forecast System Reanalysis products.[56] The chemistry mechanism is from the GEOS-Chem (v11.01) with updated isoprene nitrate uptake on aerosols.[57,58] Anthropogenic emissions are from the 2011 National Emission Inventories (2011 NEI). Biogenic emissions are calculated with the Model of Emissions of Gases and Aerosols from Nature (MEGAN) version 2.10.[59] Emissions

https://doi.org/10.1021/acs.est.1c03035
Environ. Sci. Technol. 2021, 55, 12852−12861

from biomass burning are negligible compared to anthropogenic and natural sources in the Southeast in summer[60] and are not included in the model. As shown in Figures S1 and S2 in the Supporting Information, the coincident REAM simulation results are generally within the standard deviations of observed surface and boundary-layer O_3, NO_x, NO_y (NO_x + PAN + HNO_3 in the model), CO, and HCHO concentrations. We discuss the potential effects of the model biases on simulation-derived background ozone concentrations in the result section.

2.3. Principle of the O_3−CO−HCHO Method. As discussed by Cheng et al.,[33] O_3 concentrations can be decomposed into three components: O_3 produced from anthropogenic emissions ($O_{3anthro}$), O_3 produced from biogenic emissions (O_{3bio}), and background O_3 (O_{3back}). In a region where CO is from both biogenic and anthropogenic sources but HCHO is dominated by the biogenic source, the CO−HCHO relationship can be used to compute the anthropogenic contribution to CO. As such, the three O_3 components can be separated based on eq 1, detailed derivations are discussed by Cheng et al.[33]

$$\begin{aligned} O_3 &= \frac{\Delta O_3}{\Delta CO_{anthro}}\left(CO_{total} - \frac{\Delta CO_{bio}}{\Delta HCHO_{bio}}\right. \\ &\quad \left.(HCHO_{total} - HCHO_{back}) - CO_{back}\right) \\ &\quad + \frac{\Delta O_3}{\Delta HCHO_{bio}}(HCHO_{total} - HCHO_{back}) \\ &\quad + O_{3back} \\ &= k_1(CO_{total} - CO_{back}) - (k_1k_2 - k_3) \\ &\quad (HCHO_{total} - HCHO_{back}) + O_{3back} \end{aligned} \quad (1)$$

where $k_1 = \frac{\Delta O_3}{\Delta CO_{anthro}}$, $k_2 = \frac{\Delta CO_{bio}}{\Delta HCHO_{bio}}$, $k_3 = \frac{\Delta O_3}{\Delta HCHO_{bio}}$, "anthro" denotes those from anthropogenic sources, "bio" denotes those from biogenic sources, and "total" denotes those from all sources, "back" denotes background values. The relationship of eq 1 reflects the net changes of the chemical species due to chemical production, loss, transport, and deposition. At present, we cannot separate the contribution from each process to the relationship. We choose the time window of 11 A.M. to 4 P.M. with active photochemistry over the southeastern United States where these three species are temporospatially stable (Figure S1) and the contributions from biogenic isoprene to the slope of O_3 to HCHO are dominant[33] to ensure the robustness of our analysis.

We conducted tagged tracer simulations to derive CO and HCHO from anthropogenic and biogenic sources (including emissions and chemical production) and background transport separately, while keeping model simulating other trace gases and radical concentrations, such as O_3, NO_x, and HO_x (OH and HO_2), the same as in the standard model; details are as described in the previous studies by Cheng et al.[32,33] Using tagged tracer simulation results, we can compute the values of k_1, k_2, and k_3 through least-squares regressions of O_3 and anthropogenic CO, biogenic CO and HCHO, O_3, and biogenic HCHO, respectively. We used eq 1 to compute hourly background ozone

$$\begin{aligned} O_{3back} &= O_3 - k_1(CO_{total} - CO_{back}) + (k_1k_2 - k_3) \\ &\quad (HCHO_{total} - HCHO_{back}) \end{aligned} \quad (2)$$

All variables on the right-hand side of the equation are known from standard and tagged-tracer model simulations and the background O_3 can be computed using eq 2.

When using the observations, we cannot separate species from different sources. Therefore, the values of k_1, k_2, k_3, and background concentrations of CO, HCHO, and O_3 must be determined empirically. We applied a nonlinear regression[61] of eq 1 to the SOAS and SENEX measurement data during the hours of active photochemistry between 11 A.M. and 4 P.M. The observation-derived background ozone concentrations will be compared with model results.

2.4. Modified O_3−NO_z and Other Methods to Estimate Background Ozone. In the O_3−NO_z method, the O_3 value at zero NO_z of the least-squares regression is taken as the background ozone in previous studies.[15] Figure S3 in the Supporting Information shows the scatter plot of O_3 and NO_z during SENEX (0−1 km) at 11 A.M. to 4 P.M. A least-squares regression gives an intercept value of 29.8 ppbv. The scatter of the data is fairly large reflecting in part the varying degree of impact from regional emissions in the observations. The much higher ozone concentrations of the red than black data points are likely a reflection of regional ozone enhancements due to the emissions of ozone precursors in the region. In order to derive the clean-background ozone estimates, we did a second least-squares regression for the data, of which the ozone values are less than $a + b[NO_z] - 0.5\sigma$, where a, b, and σ are the intercept, slope, standard deviation of the first least-squares regression. For a Gaussian distribution, the data below half of the standard deviation are the lower 31 percentile data. Its mean value is close to the lower 1-σ (1 standard deviation) value. Figure S3 shows that the second regression line is close to the lower 1-σ line of the first regression. Because the data distribution is not ideally Gaussian, the lower 1-σ line of the first regression is slightly below the second regression line using the lower 31 percentile data. We refer to this method as the 1-σ O_3−NO_z method. Using this method, we obtain an ozone background value of 21.3 ± 6.9 ppbv for the boundary layer (0−1 km) during SENEX.

When using the zero-emission method,[7] we carried out a sensitivity simulation in which all anthropogenic emissions are turned off and the simulated O_3 concentrations are taken as the background. This method cannot be applied to the observation data. The 5th percentile method,[34] on the other hand, can be applied to both observation and model data, in which the 5th percentile O_3 concentrations are taken as the background. In order to compare to the results using the O_3−CO−HCHO method, observation and model data from 11 A.M. to 4 P.M. were analyzed.

In this study, we seek to compute objectively the clean-background ozone as the portion of ozone that does not have chemical signatures showing ozone production from anthropogenic or natural emissions of ozone precursors based on the relationship of O_3−CO−HCHO. In the comparison to the results using other methods, we adapted the O_3−NO_z method to the 1-σ O_3−NO_z method for clean air masses which are not affected by regional emissions. We applied the 5th percentile method to the entire analysis data set such that the results are independent from site or data selection.

https://doi.org/10.1021/acs.est.1c03035
Environ. Sci. Technol. 2021, 55, 12852−12861

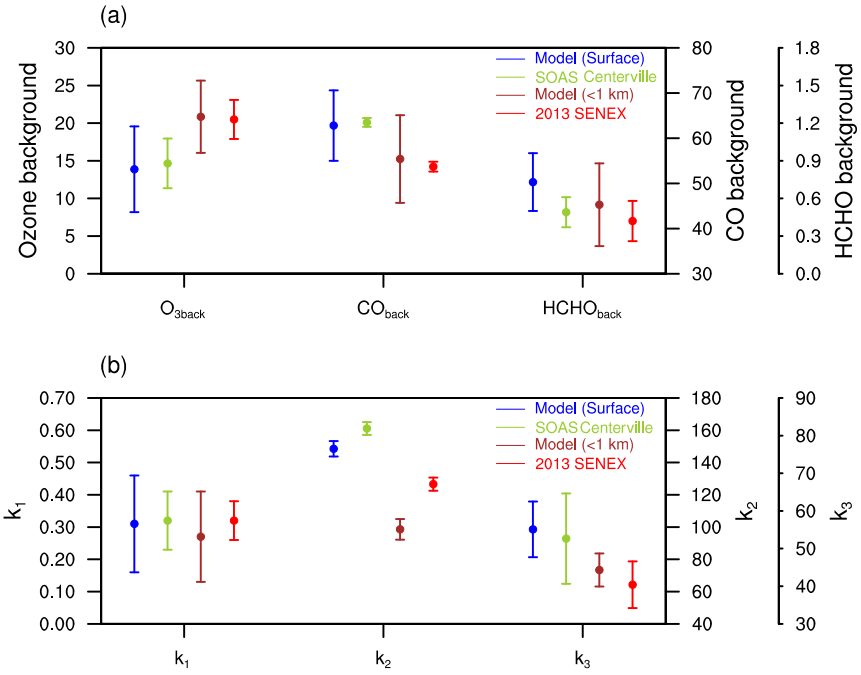

Figure 1. Estimates of the six parameters (O_{3back}, CO_{back}, $HCHO_{back}$, k_1, k_2, and k_3) in eqs 1 and 2 calculated using the observations during the 2013 SOAS Centreville campaign (green), 0−1 km measurements during the 2013 SENEX aircraft campaign (red), and the corresponding model results (blue for SOAS and brown for SENEX 0−1 km). Standard deviations of the estimates are shown by vertical bars. Daytime data from 11 A.M. to 4 P.M. are used.

3. RESULTS AND DISCUSSION

3.1. Background Ozone Concentrations Derived from SOAS and SENEX Observations and Corresponding Model Simulations Using Different Methods. We applied different methods, tagged-tracer simulations and nonlinear regression method, to solve eq 2 and derive the background ozone using simulated and observed data during SOAS and SENEX campaign as observation data cannot distinguish tracer gases from different sources. We first discuss the results using the O_3−CO−HCHO method. Figure 1 shows the derived background values of O_3, CO, and HCHO, and the slopes of k_1, k_2, and k_3, in eq 2, based on the observation and corresponding model data. The relationships between O_3, CO, and HCHO during the SOAS and SENEX campaign are shown in Figure S4. The correlations between O_3 and CO are tighter than those of O_3 or CO with HCHO partly because the lifetime of HCHO is shorter than O_3 and CO. The general positive slops of O_3 to CO or HCHO, and CO to HCHO reflect photochemical productions of O_3, CO, and HCHO. Because the lifetimes of CO and O_3 are long enough for significant regional transport, both transport and chemistry errors in the model can lead to deviations from the observations and the transport effect is larger for CO. Detailed analysis requires another study and is beyond the scope of this work.

We use the regression uncertainty ranges of six parameters shown in Figure 1 to indicate the goodness of the nonlinear regression results using the observation data. The model uncertainty in Figure 1, on the other hand, is the standard deviation of calculated hourly background ozone values. In a nonlinear regression of the observation data, the traditional R^2 value, the fraction of the total variance explained by the regression model, cannot be used to assess the goodness-of-fit of the nonlinear model because the total variance does not equal to the sum of explained variance and error variance and the R^2 value is not in the range of 0−100%.[62] The parameter uncertainties reflect the effects of the independent variables and random data variations on the regression model.[63] The small standard errors of the six parameters shown in the Figure 1 indicate the robustness of the regression results.

Observed and model-derived parameters are generally in good agreement; the one standard deviation error ranges of the parameters mostly overlap. The exception is that the model derived k_2 values are 10−30% lower than the observations. It may imply that either the CO yield is low or the net HCHO yield is high in the simulated isoprene chemical mechanism although regional transport of CO may also have an impact on the model bias. While additional measurements and modeling are necessary to infer the biases of CO and HCHO yields in the model isoprene oxidation mechanism, the analysis here provides an additional method to make use of the observation data to test the model chemical mechanism. The reasons for the observed and simulated 20−30% lower k_2 values at Centreville than the SENEX data are unclear. The large vertical gradients of NO_x, CO, and HCHO in the boundary layer (Figure S2), the nonlinear isoprene chemistry, and the sampling differences in time and location are among the factors complicating a quantitative analysis. Because CO has a long lifetime, the slope value of k_1 can be thought of as a measure of the O_3 production efficiency by anthropogenic NO_x during isoprene oxidation. The fairly good agreement between the model and observation results provides support for using the model to simulate the change of O_3 due to anthropogenic emissions. The slope value of k_3 indicates the change of O_3 relative to HCHO during isoprene oxidation. The value is much larger than 1 largely because of a much longer lifetime of O_3 than HCHO.

The observation and model-derived background levels of CO (50−65 ppbv) and HCHO (0.5−0.7 ppbv) are largely due

https://doi.org/10.1021/acs.est.1c03035
Environ. Sci. Technol. 2021, 55, 12852−12861

to the oxidation of CH_4 and comparable to results of Cheng et al.[33] The derived CO and HCHO background values using observations have lower uncertainties than the model results due largely to the difference of the calculation method. The purpose of a regression model is to minimize the uncertainties of regression function and parameters. Therefore, the range of the uncertainty reflects not just how well the regression model fits the data but also the optimization in the parameter space. The model background CO and HCHO mean and standard deviation values are computed directly using tagged tracer simulations. The standard deviations reflect the spatiotemporal variations of the model data. There is no optimization process to minimize the uncertainties in the model estimates. In other words, all terms on the right-hand side of eq 2 are known from the model results, but they are unknown in the observation data. The higher degree of freedom in the nonlinear regression optimization of the observation data results in lower uncertainty estimates in the parameter space.

Using the O_3−CO−HCHO method, we estimate background ozone concentrations of 14.7 ± 3.3 and 20.5 ± 2.6 ppbv for SOAS and SENEX observations, respectively. The corresponding values for the model results are 13.9 ± 5.7 and 20.8 ± 4.8 ppbv, ∼1 ppbv difference compared to the observation-based values but well within the standard deviations of the estimates. On average, the SENEX background ozone at 0−1 km is ∼6 ppbv higher than that of SOAS near the surface in both observations and models, reflecting in part the effect of dry deposition loss of ozone at the surface. The excellent agreement between model and observation values reflects in part the robustness of this method.

3.2. Comparisons of Background Ozone Estimates Using the O_3−CO−HCHO Method to the Previous Methods. The comparison results are summarized in Figure 2. Among the previously used methods, the modified 1-σ O_3−NO_z method is the most similar to the O_3−CO−HCHO method, both of which rely on tracer correlations in the estimation of a clean-background ozone. However, the latter new method makes use of the full observation data sets, while the former uses the lower 31 percentile data. The estimated background ozone concentrations are 18.7 ± 6.5 and 21.3 ± 6.9 ppbv, respectively, for SOAS (surface) and SENEX (0−1 km) observations in the 1-σ O_3−NO_z method. The corresponding model estimates are 19.9 ± 6.4 and 21.0 ± 7.6 ppbv. The uncertainties of the observation-based estimates are larger than the O_3−CO−HCHO method, in part because smaller sized data sets are used and in part because the deviations from the regression lines are larger. The small increase of background ozone from the surface to 1 km can be found both in the model and observation data. Overall, the background concentrations derived using the 1-σ O_3−NO_z method are similar to the O_3−CO−HCHO results within the boundary layer, but higher by about 40% than the O_3−CO−HCHO method at the surface. It implies that the 1-σ threshold we chosen to indicate the clean-background ozone may bias high at the surface. We can reduce the high biases using the 1-σ O_3−NO_z method by increasing the cut-off threshold of 0.5σ_z from the regression line. If it is increased to 1σ_z from the regression line, we would use about 17% of the data set. Because there is no physically based criterion for determining the cut-off threshold, the decision is statistical in nature. A small fraction of the data population calls into the question of the data representativeness. For example, if the 1σ_z cut-off line is used in Figure S3, only about 20 data points are left for NO_z > 2.5 ppbv, not representative of the original data.

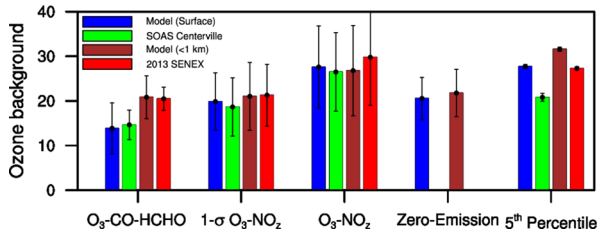

Figure 2. Estimated background ozone concentrations for the observations and corresponding model results during SOAS (surface) and SENEX (0−1 km). Standard deviations of the estimates are shown by vertical bars. Daytime data from 11 A.M. to 4 P.M. are used.

Compared to the 1-σ O_3−NO_z method, the O_3−NO_z method gives 25−40% higher estimates, which are 26.5 ± 8.8 and 29.8 ± 10.8 ppbv for SOAS and SENEX observations, respectively, and the corresponding values are 27.6 ± 9.2 and 26.8 ± 10.1 ppbv in the model. The results are consistent with the discussion of Figure S3 in Section 2.4. The data scattering and higher intercepts of the O_3−NO_z regression reflect the variability of ozone production in the sampled air masses. For the purpose of deriving the clean-background ozone in this work, the 1-σ O_3−NO_z method is more appropriate.

The zero-emission method is for model only. Using the model data corresponding to the observations, we estimate background ozone concentrations of 20.6 ± 4.7 and 21.8 ± 5.3 ppbv for model data corresponding to the SOAS (surface) and SENEX (0−1 km) observations, respectively, which are 3−48% higher than the estimates using the O_3−CO−HCHO method. Fiore et al.[6] found a mean afternoon background ozone of 15−30 ppbv in the eastern United States using the zero-emission method. Our zero-emission results are similar and in the middle range of their results. The higher zero-emission background ozone concentrations than those derived using the O_3−CO−HCHO method or the 1-σ O_3−NO_z method reflect two processes. In zero-emission simulations, all anthropogenic emissions are zeroed out but natural emissions, such as soil and lightning NO_x, are included, leading to chemical production of ozone by regional sources. In the O_3−CO−HCHO methods, anthropogenic and natural precursors are treated in the same manner and the derived background ozone is presumed to be independent of both anthropogenic and natural sources in the region. Another reason is that the HO_2 radical promotes ozone production and loss through the reactions of HO_2 + NO and HO_2 + O_3, respectively. In a photochemically active boundary layer with anthropogenic and natural emissions, background ozone transported from remote regions has a shorter lifetime and lower concentrations due in part to higher HO_2 concentrations compared to a photochemical environment without anthropogenic emissions and low ozone concentrations. For this chemical-nonlinearity reason, we expect a lower ozone background in the daytime than nighttime and in summer than the other seasons.

The 5th percentile method yields higher estimates of background ozone in general, 20.8 ± 0.9 and 27.3 ± 0.3 ppbv for SOAS (surface) and SENEX (0−1 km) observations, respectively. The uncertainties, which are estimated using 10,000 times bootstraps, are considerably less than other methods. The corresponding model results are 27.7 ± 0.5 and 31.6 ± 0.6 ppbv. The lower value based on the SOAS

https://doi.org/10.1021/acs.est.1c03035
Environ. Sci. Technol. 2021, 55, 12852−12861

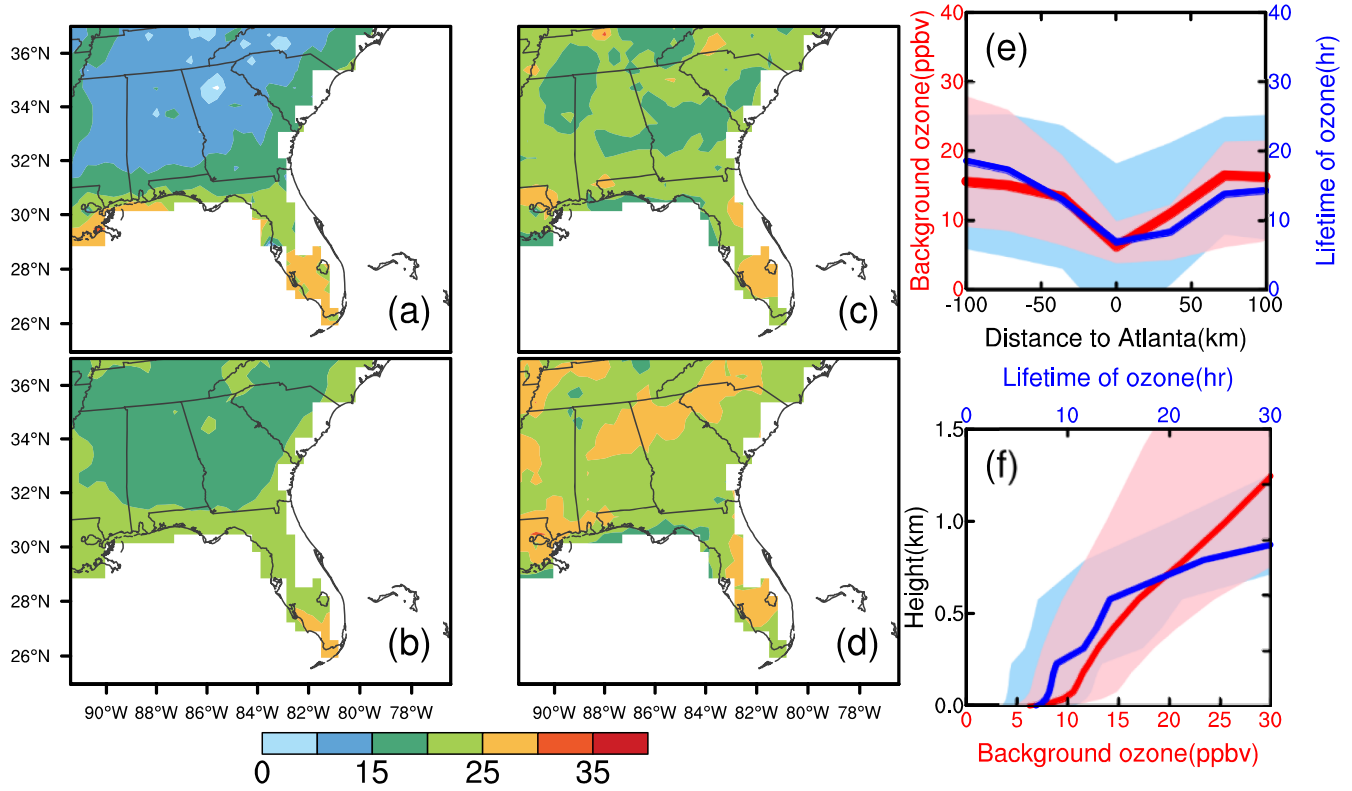

Figure 3. Estimates of background ozone distribution for the SE in the summer of 2013 using the O_3−CO−HCHO (a), zero-emission (b), 1-σ O_3−NO_z (c), and 5th percentile (d) methods. Also shown are the dependence of background ozone derived from the O_3−CO−HCHO method (red) and the lifetime of ozone due to chemical loss and dry deposition (blue) on the distance from Atlanta (e) and altitude (f). The surface-layer model results in grid cells to the left and right of Atlanta (at the same latitude) are used in (e). The results for Atlanta grid cells are used in (f). Solid lines show the averages and shaded areas show standard deviations. Hourly data from 11 A.M. to 4 P.M. are used.

observations than SENEX measurements could reflect periods of low surface ozone when the observation site was strongly affected by transport from the Gulf of Mexico, and lower modeled background values imply the effect of which was underestimated by the model. These estimates are 40−100% higher than the estimates using the O_3−CO−HCHO method. Wilson et al.[34] selected 5th percentile as the background ozone value based on 397 ground sites representing not only "baseline" sites but also rural, suburban, and urban sites. The implicit 5th percentile selection as the background ozone level can be problematic with higher or lower estimation under different pollution environments. Also, the statistical and physical reasons of using a specific percentile as the background level are not apparent.

Among the various estimates, the O_3−CO−HCHO method gives the largest difference between the SOAS surface site and the SENEX 0−1 km background ozone concentrations. The 5th percentile method also shows significantly lower ozone concentrations for SOAS surface background ozone reflecting in part the effect of ozone dry deposition to the surface. The zero-emission method shows less difference than the O_3−CO−HCHO method. The reason is related to a shorter photochemical lifetime of background ozone with more active photochemistry driven by anthropogenic emissions, which we will discuss in more detail in the next section. The regular and 1-σ O_3−NO_z methods give a somewhat lower SOAS surface than SENEX (0−1 km) background ozone concentrations, but the difference is well within the standard deviations. Unlike the other methods, the O_3−NO_z methods are also affected by dry deposition of HNO_3 to the surface, the rate of which is much faster than ozone, thereby masking the effect of ozone dry deposition to the surface.

3.3. Background Ozone Distribution in the Southeast. We compile previous background ozone estimates for the United States in Table S2 in the Supporting Information.[6−8,10−13,15,20,21,64−70] The previous observation and model studies suggest a background ozone of 15−40 ppbv for the eastern United States and higher levels for the western United States. The estimates using the new O_3−CO−HCHO method for SOAS and SENEX (Figure 2) are at the very low end of the previous estimates similar to the 1-σ O_3−NO_z results. Zero-emission results are in the middle range while the 5th percentile and O_3−NO_z results are more comparable to the previous studies.

To further compare to the previous studies, we apply the O_3−CO−HCHO and other methods to derive background ozone distributions of the Southeast for the summer (June−August) of 2013 using model results. The O_3−CO−HCHO method can only be applied to the region where HCHO is dominated by biogenic isoprene emissions.[32,33] The other three methods are applied to the model results over the United States (Figure S5). The general distributions are similar to previous studies,[8,10,68] showing that background ozone is about 20 ppbv higher in the West than the East.

Figure 3 compares the estimated background ozone distributions in the Southeast. The O_3−CO−HCHO and zero-emission methods give the most consistent distribution feature: background ozone concentrations decrease from the coastlines to inland regions. In comparison, the results from the 1-σ O_3−NO_z and 5th percentile methods show larger and

https://doi.org/10.1021/acs.est.1c03035
Environ. Sci. Technol. 2021, 55, 12852−12861

different spatial variations in land areas. One difference between the O_3−CO−HCHO and zero-emission methods is apparent for the Atlanta region. The lifetime of ozone is determined by photochemical loss and dry deposition of ozone. In the O_3−CO−HCHO method, metropolitan areas yield a lower ozone background because active photochemistry due to anthropogenic emissions decreases the lifetime of background ozone (Figure S6) and dry deposition lifetime have a lesser impact on background ozone (Figure S7); the chemical lifetime of ozone is about 7 h in Atlanta in comparison to 18 h at Centreville. In the zero-emission simulation, on the other hand, dry deposition loss becomes more important because the chemical lifetime of background ozone is longer with zero anthropogenic emissions. The background ozone level of zero-emission is estimated higher in Atlanta than surrounding regions partly because of lower dry deposition loss of ozone in urban (~0.4 cm s^{-1} in Atlanta) than surrounding forest regions (0.6−0.7 cm s^{-1}) in the model (Figure S8).

Figure 3 shows that the background ozone concentration derived from the O_3−CO−HCHO method around Atlanta correlates well with ozone lifetime. Near the surface, background concentrations of ozone and its lifetime are lower in urban than rural regions. In the vertical direction, because most of anthropogenic emissions occur near the surface, the more active photochemistry driven by anthropogenic emissions tends to shorten ozone chemical lifetime near the surface (Figure S7). Therefore, changing ozone lifetime due to anthropogenic emissions and dry deposition to the surface tends to lead to increasing background ozone from urban to rural regions and from the surface to higher altitude.

The O_3−CO−HCHO method gives the lowest estimates of background ozone near the surface at 10−15 ppbv in the inland SE region, compared to 15−20, 15−25, and 20−30 ppbv in the zero-emission, 1-σ O_3−NO_z, and 5th percentile methods, respectively. Much of the differences are related to the interpretation of the results. The highest estimates by the 5th percentile method suggest that the effects of anthropogenic emissions are not entirely filtered out in this method. Downwind from an urban region, the estimate tends to be higher because ozone concentrations are higher than surrounding forest regions. The 1-σ O_3−NO_z estimates tend to have larger variations than other methods partly because HNO_3 is removed by dry and wet deposition. The effect of dry deposition is largest near the surface. The effect of wet deposition has large variations and is sporadic depending on convection, precipitation, and cloud, contributing to the uncertainties of this method. The zero-emission method does not consider the chemical nonlinearity effect on background ozone and does not exclude the portion of ozone produced from natural emissions of ozone precursors.

The O_3−CO−HCHO method attempts to exclude the effects of anthropogenic and natural emissions of ozone precursors in the region on background ozone estimates. This method can be applied to both observation and model simulation data, and the results are robust. The spatial distribution is what we expect, and it is the only method that shows lower background ozone concentrations in urban regions (Figure 3). This method provides the means to compute the clean-background ozone as the portion of ozone that does not have chemical signatures showing ozone production from anthropogenic or natural emissions of ozone precursors. Compared to operationally defined background or baseline ozone levels, such as using the ozone measurements from a remote coastal "background" site which may still be affected by ozone produced from upwind polluted regions, the definition we used in this study does not rely on prior assumptions on factors such as the varying impacts of upwind polluted regions. It is therefore not surprising that the clean ozone background is lower than that computed using the other methods we tried or in comparison to previous studies, which still has a regional component. We suggest that this clean ozone background computed using the O_3−CO−HCHO method provides an objective basis for evaluating and interpreting the higher baseline ozone levels derived using operational definitions of ozone background.

The estimated clean background ozone tends to increase from urban to rural regions and from the surface to higher altitude due to changing ozone lifetime driven by anthropogenic emissions and dry deposition to the surface. A limitation of this method is that it does not discriminate anthropogenic from natural emissions. By comparing to the zero-emission method, the effect of natural emissions can be estimated, however, at ~5 ppbv in the Southeast (Figure S9). Unlike the model-only zero-emission method, the model-based background ozone estimates using O_3−CO−HCHO method can be evaluated using observations such as SOAS and SENEX. The lower summertime background ozone estimates using the newly developed O_3−CO−HCHO method than previous studies highlight the importance of the contributions by natural emissions to ozone and the necessity to control anthropogenic emissions in ozone nonattainment areas of the Southeast.

More generally for future regional ozone studies, we suggest that background ozone be separated into two components: (1) a zero-chemical-signature background in line with what we established in this study using the O_3−CO−HCHO method and (2) a regional background ozone that still has chemical signatures associated with ozone-precursor relationships. Such a separation of the ozone background components enables the quantitative analysis and discussion of the much more variable regional effects separately from an objectively defined less variable clean ozone background.

■ ASSOCIATED CONTENT

Supporting Information

The Supporting Information is available free of charge at https://pubs.acs.org/doi/10.1021/acs.est.1c03035.

Descriptions of tagged tracer model; additional details about 2013 SOAS and SENEX observations; reviews of previous background ozone estimates; estimates of U.S. background ozone using different methods; chemical lifetime and dry deposition velocity distributions over the SE; and comparisons of background ozone between the O_3−CO−HCHO and zero-emission methods over the SE for the summer of 2013 (PDF)

■ AUTHOR INFORMATION

Corresponding Author

Yuhang Wang − *School of Earth and Atmospheric Sciences, Georgia Institute of Technology, Atlanta, Georgia 30332, United States;* orcid.org/0000-0002-7290-2551; Phone: +1 (404) 894 3995; Email: yuhang.wang@eas.gatech.edu; Fax: +1 (404) 894 5638

https://doi.org/10.1021/acs.est.1c03035
Environ. Sci. Technol. 2021, 55, 12852−12861

Authors

Qiyang Yan − *School of Earth and Atmospheric Sciences, Georgia Institute of Technology, Atlanta, Georgia 30332, United States;* orcid.org/0000-0003-0799-2156

Ye Cheng − *School of Earth and Atmospheric Sciences, Georgia Institute of Technology, Atlanta, Georgia 30332, United States*

Jianfeng Li − *School of Earth and Atmospheric Sciences, Georgia Institute of Technology, Atlanta, Georgia 30332, United States;* Present Address: Now at atmospheric sciences and global change division, Pacific Northwest National Laboratory, Richland, Washington 99354, United States; orcid.org/0000-0002-1091-9753

Complete contact information is available at: https://pubs.acs.org/10.1021/acs.est.1c03035

Notes

The authors declare no competing financial interest.

■ ACKNOWLEDGMENTS

This work was supported by the NASA ACMAP Program. We thank the 2013 SOAS Centreville field team including Eric Edgerton for O_3, NO_y, NO, NO_2, and CO observations and Frank Keutsch for the HCHO data. We also thank Ilana Pollack and Thomas Ryerson for the 2013 SENEX O_3, NO_y, NO, NO_2 data, John Holloway for SENEX CO data, and Thomas Hanisco for SENEX HCHO data.

■ REFERENCES

(1) *National Ambient Air Quality Standards for Ozone*; U.S. Environmental Protection Agency: Triangle Park, NC, 2015; https://www.govinfo.gov/content/pkg/FR-2020-08-14/pdf/2020-15453.pdf.

(2) Zhang, Y.; Wang, Y. Climate driven ground-level ozone extreme in the fall over the Southeast United States. *Proc. Natl. Acad. Sci.* **2016**, *113*, 10025−10030.

(3) Cooper, O. R.; Gao, R. S.; Tarasick, D.; Leblanc, T.; Sweeney, C. Long-term ozone trends at rural ozone monitoring sites across the United States, 1990−2010. *J. Geophys. Res.: Atmos.* **2012**, *117*, D22.

(4) Simon, H.; Reff, A.; Wells, B.; Xing, J.; Frank, N. Ozone trends across the United States over a period of decreasing NO_x and VOC emissions. *Environ. Sci. Technol.* **2015**, *49*, 186−195.

(5) Lin, M.; Horowitz, L. W.; Payton, R.; Fiore, A. M.; Tonnesen, G. US surface ozone trends and extremes from 1980 to 2014: quantifying the roles of rising Asian emissions, domestic controls, wildfires, and climate. *Atmos. Chem. Phys.* **2017**, *17*, 2943−2970.

(6) Fiore, A. M.; Jacob, D. J.; Bey, I.; Yantosca, R. M.; Field, B. D.; Fusco, A. C.; Wilkinson, J. G. Background ozone over the United States in summer: Origin, trend, and contribution to pollution episodes. *J. Geophys. Res.: Atmos.* **2002**, *107*, ACH-11.

(7) Fiore, A.; Jacob, D. J.; Liu, H.; Yantosca, R. M.; Fairlie, T. D.; Li, Q. Variability in surface ozone background over the United States: Implications for air quality policy. *J. Geophys. Res.: Atmos.* **2003**, *108*, 4787.

(8) Zhang, L.; Jacob, D. J.; Downey, N. V.; Wood, D. A.; Blewitt, D.; Carouge, C. C.; van Donkelaar, A.; Jones, D. B. A.; Murray, L. T.; Wang, Y. Improved estimate of the policy-relevant background ozone in the United States using the GEOS-Chem global model with 1/2×2/3 horizontal resolution over North America. *Atmos. Environ.* **2011**, *45*, 6769−6776.

(9) Lin, M.; Fiore, A. M.; Horowitz, L. W.; Cooper, O. R.; Naik, V.; Holloway, J.; Johnson, B. J.; Middlebrook, A. M.; Oltmans, S. J.; Pollack, I. B.; Ryerson, T. B. Transport of Asian ozone pollution into surface air over the western United States in spring. *J. Geophys. Res.: Atmos.* **2012**, *117*, D00V07.

(10) Emery, C.; Jung, J.; Downey, N.; Johnson, J.; Jimenez, M.; Yarwood, G.; Morris, R. Regional and global modeling estimates of policy relevant background ozone over the United States. *Atmos. Environ.* **2012**, *47*, 206−217.

(11) Fiore, A. M.; Oberman, J. T.; Lin, M. Y.; Zhang, L.; Clifton, O. E.; Jacob, D. J.; Naik, V.; Horowitz, L. W.; Pinto, J. P.; Milly, G. P. Estimating North American background ozone in US surface air with two independent global models: Variability, uncertainties, and recommendations. *Atmos. Environ.* **2014**, *96*, 284−300.

(12) Lefohn, A. S.; Emery, C.; Shadwick, D.; Wernli, H.; Jung, J.; Oltmans, S. J. Estimates of background surface ozone concentrations in the United States based on model-derived source apportionment. *Atmos. Environ.* **2014**, *84*, 275−288.

(13) Dolwick, P.; Akhtar, F.; Baker, K. R.; Possiel, N.; Simon, H.; Tonnesen, G. Comparison of background ozone estimates over the western United States based on two separate model methodologies. *Atmos. Environ.* **2015**, *109*, 282−296.

(14) Jaffe, D. A.; Cooper, O. R.; Fiore, A. M.; Henderson, B. H.; Tonnesen, G. S.; Russell, A. G.; Henze, D. K.; Langford, A. O.; Lin, M.; Moore, T. Scientific assessment of background ozone over the US: Implications for air quality management. *Elementa* **2018**, *6*, 56.

(15) Altshuller, A. P.; Lefohn, A. S. Background ozone in the planetary boundary layer over the United States. *J. Air Waste Manage. Assoc.* **1996**, *46*, 134−141.

(16) Vingarzan, R. A review of surface ozone background levels and trends. *Atmos. Environ.* **2004**, *38*, 3431−3442.

(17) Cooper, O. R.; Langford, A. O.; Parrish, D. D.; Fahey, D. W. Challenges of a lowered US ozone standard. *Science* **2015**, *348*, 1096−1097.

(18) Liu, S. C.; Trainer, M.; Fehsenfeld, F. C.; Parrish, D. D.; Williams, E. J.; Fahey, D. W.; Hübler, G.; Murphy, P. C. Ozone production in the rural troposphere and the implications for regional and global ozone distributions. *J. Geophys. Res.: Atmos.* **1987**, *92*, 4191−4207.

(19) Kleinman, L. I.; Daum, P. H.; Lee, Y. N.; Nunnermacker, L. J.; Springston, S. R.; Weinstein-Lloyd, J.; Rudolph, J. Ozone production efficiency in an urban area. *J. Geophys. Res.: Atmos.* **2002**, *107*, ACH-23.

(20) Hirsch, A. I.; Munger, J. W.; Jacob, D. J.; Horowitz, L. W.; Goldstein, A. H. Seasonal variation of the ozone production efficiency per unit NO_x at Harvard Forest, Massachusetts. *J. Geophys. Res.: Atmos.* **1996**, *101*, 12659−12666.

(21) Trainer, M.; Parrish, D. D.; Buhr, M. P.; Norton, R. B.; Fehsenfeld, F. C.; Anlauf, K. G.; Bottenheim, J. W.; Tang, Y. Z.; Wiebe, H. A.; Roberts, J. M.; Tanner, R. L.; Newman, L.; Bowersox, V. C.; Meagher, J. F.; Olszyna, K. J.; Rodgers, M. O.; Wang, T.; Berresheim, H.; Demerjian, K. L.; Roychowdhury, U. K. Correlation of ozone with NO_y in photochemically aged air. *J. Geophys. Res.: Atmos.* **1993**, *98*, 2917−2925.

(22) Parrish, D. D.; Holloway, J. S.; Trainer, M.; Murphy, P. C.; Fehsenfeld, F. C.; Forbes, G. L. Export of North American ozone pollution to the north Atlantic Ocean. *Science* **1993**, *259*, 1436−1439.

(23) Chin, M.; Jacob, D. J.; Munger, J. W.; Parrish, D. D.; Doddridge, B. G. Relationship of ozone and carbon monoxide over North America. *J. Geophys. Res.: Atmos.* **1994**, *99*, 14565−14573.

(24) Buhr, M.; Sueper, D.; Trainer, M.; Goldan, P.; Kuster, B.; Fehsenfeld, F.; Kok, G.; Shillawski, R.; Schanot, A. Trace gas and aerosol measurements using aircraft data from the North Atlantic Regional Experiment (NARE 1993). *J. Geophys. Res.: Atmos.* **1996**, *101*, 29013−29027.

(25) Parrish, D. D.; Trainer, M.; Holloway, J. S.; Yee, J. E.; Warshawsky, M. S.; Fehsenfeld, F. C.; Forbes, G. L.; Moody, J. L. Relationships between ozone and carbon monoxide at surface sites in the North Atlantic region. *J. Geophys. Res.: Atmos.* **1998**, *103*, 13357−13376.

(26) Cárdenas, L. M.; Austin, J. F.; Burgess, R. A.; Clemitshaw, K. C.; Dorling, S.; Penkett, S. A.; Harrison, R. M. Correlations between CO, NO_y, O_3 and non-methane hydrocarbons and their relationships

with meteorology during winter 1993 on the North Norfolk Coast, UK. *Atmos. Environ.* **1998**, *32*, 3339−3351.
(27) Cooper, O. R.; Moody, J. L.; Parrish, D. D.; Trainer, M.; Holloway, J. S.; Hübler, G.; Fehsenfeld, F. C.; Stohl, A. Trace gas composition of midlatitude cyclones over the western North Atlantic Ocean: A seasonal comparison of O_3 and CO. *J. Geophys. Res.: Atmos.* **2002**, *107*, ACH-2.
(28) Cooper, O. R.; Moody, J. L.; Parrish, D. D.; Trainer, M.; Ryerson, T. B.; Holloway, J. S.; Hübler, G.; Fehsenfeld, F. C.; Evans, M. J. Trace gas composition of midlatitude cyclones over the western North Atlantic Ocean: A conceptual model. *J. Geophys. Res.: Atmos.* **2002**, *107*, ACH-1.
(29) Honrath, R. E.; Owen, R. C.; Val Martin, M.; Reid, J. S.; Lapina, K.; Fialho, P.; Dziobak, M. P.; Kleissl, J.; Westphal, D. L. Regional and hemispheric impacts of anthropogenic and biomass burning emissions on summertime CO and O_3 in the North Atlantic lower free troposphere. *J. Geophys. Res.: Atmos.* **2004**, *109*, D24310.
(30) Mao, H.; Talbot, R. O_3 and CO in New England: Temporal variations and relationships. *J. Geophys. Res.: Atmos.* **2004**, *109*, D21304.
(31) Huntrieser, H.; Heland, J.; Schlager, H.; Forster, C.; Stohl, A.; Aufmhoff, H.; Arnold, F.; Scheel, H. E.; Campana, M.; Gilge, S.; Eixmann, R. Intercontinental air pollution transport from North America to Europe: Experimental evidence from airborne measurements and surface observations. *J. Geophys. Res.: Atmos.* **2005**, *110*, D01305.
(32) Cheng, Y.; Wang, Y.; Zhang, Y.; Chen, G.; Crawford, J. H.; Kleb, M. M.; Diskin, G. S.; Weinheimer, A. J. Large biogenic contribution to boundary layer O_3-CO regression slope in summer. *Geophys. Res. Lett.* **2017**, *44*, 7061−7068.
(33) Cheng, Y.; Wang, Y.; Zhang, Y.; Crawford, J. H.; Diskin, G. S.; Weinheimer, A. J.; Fried, A. Estimator of surface ozone using formaldehyde and carbon monoxide concentrations over the eastern United States in summer. *J. Geophys. Res.: Atmos.* **2018**, *123*, 7642−7655.
(34) Wilson, R. C.; Fleming, Z. L.; Monks, P. S.; Clain, G.; Henne, S.; Konovalov, I. B.; Szopa, S.; Menut, L. Have primary emission reduction measures reduced ozone across Europe? An analysis of European rural background ozone trends 1996−2005. *Atmos. Chem. Phys.* **2012**, *12*, 437−454.
(35) Carlton, A. G.; de Gouw, J.; Jimenez, J. L.; Ambrose, J. L.; Attwood, A. R.; Brown, S.; Baker, K. R.; Brock, C.; Cohen, R. C.; Edgerton, S.; Farkas, C. M.; Farmer, D.; Goldstein, A. H.; Gratz, L.; Guenther, A.; Hunt, S.; Jaeglé, L.; Jaffe, D. A.; Mak, J.; McClure, C.; Nenes, A.; Nguyen, T. K.; Pierce, J. R.; de Sa, S.; Selin, N. E.; Shah, V.; Shaw, S.; Shepson, P. B.; Song, S.; Stutz, J.; Surratt, J. D.; Turpin, B. J.; Warneke, C.; Washenfelder, R. A.; Wennberg, P. O.; Zhou, X. The Southeast Atmosphere Studies (SAS): coordinated investigation and discovery to answer critical questions about fundamental atmospheric processes. *Bull. Am. Meteorol. Soc.* **2018**, *99*, 547−567.
(36) Mao, J.; Carlton, A.; Cohen, R. C.; Brune, W. H.; Brown, S. S.; Wolfe, G. M.; Jimenez, J. L.; Pye, H. O. T.; Lee Ng, N.; Xu, L.; McNeill, V. F.; Tsigaridis, K.; McDonald, B. C.; Warneke, C.; Guenther, A.; Alvarado, M. J.; de Gouw, J.; Mickley, L. J.; Leibensperger, E. M.; Mathur, R.; Nolte, C. G.; Portmann, R. W.; Unger, N.; Tosca, M.; Horowitz, L. W. Southeast Atmosphere Studies: learning from model-observation syntheses. *Atmos. Chem. Phys.* **2018**, *18*, 2615−2651.
(37) Feiner, P. A.; Brune, W. H.; Miller, D. O.; Zhang, L.; Cohen, R. C.; Romer, P. S.; Goldstein, A. H.; Keutsch, F. N.; Skog, K. M.; Wennberg, P. O.; Nguyen, T. B.; Teng, A. P.; DeGouw, J.; Koss, A.; Wild, R. J.; Brown, S. S.; Guenther, A.; Edgerton, E.; Baumann, K.; Fry, J. L. Testing atmospheric oxidation in an Alabama forest. *J. Atmos. Sci.* **2016**, *73*, 4699−4710.
(38) Warneke, C.; Trainer, M.; de Gouw, J. A.; Parrish, D. D.; Fahey, D. W.; Ravishankara, A. R.; Middlebrook, A. M.; Brock, C. A.; Roberts, J. M.; Brown, S. S.; Neuman, J. A.; Lerner, B. M.; Lack, D.; Law, D.; Hübler, G.; Pollack, I.; Sjostedt, S.; Ryerson, T. B.; Gilman, J. B.; Liao, J.; Holloway, J.; Peischl, J.; Nowak, J. B.; Aikin, K. C.; Min, K.-E.; Washenfelder, R. A.; Graus, M. G.; Richardson, M.; Markovic, M. Z.; Wagner, N. L.; Welti, A.; Veres, P. R.; Edwards, P.; Schwarz, J. P.; Gordon, T.; Dube, W. P.; McKeen, S. A.; Brioude, J.; Ahmadov, R.; Bougiatioti, A.; Lin, J. J.; Nenes, A.; Wolfe, G. M.; Hanisco, T. F.; Lee, B. H.; Lopez-Hilfiker, F. D.; Thornton, J. A.; Keutsch, F. N.; Kaiser, J.; Mao, J.; Hatch, C. D. Instrumentation and measurement strategy for the NOAA SENEX aircraft campaign as part of the Southeast Atmosphere Study 2013. *Atmos. Meas. Tech.* **2016**, *9*, 3063−3093.
(39) Hansen, D. A.; Edgerton, E. S.; Hartsell, B. E.; Jansen, J. J.; Kandasamy, N.; Hidy, G. M.; Blanchard, C. L. The southeastern aerosol research and characterization study: Part 1— Overview. *J. Air Waste Manage. Assoc.* **2003**, *53*, 1460−1471.
(40) Hottle, J. R.; Huisman, A. J.; DiGangi, J. P.; Kammrath, A.; Galloway, M. M.; Coens, K. L.; Keutsch, F. N. A laser induced fluorescence-based instrument for in-situ measurements of atmospheric formaldehyde. *Environ. Sci. Technol.* **2009**, *43*, 790−795.
(41) Holloway, J. S.; Jakoubek, R. O.; Parrish, D. D.; Gerbig, C.; Volz-Thomas, A.; Schmitgen, S.; Fried, A.; Wert, B.; Henry, B.; Drummond, J. R. Airborne intercomparison of vacuum ultraviolet fluorescence and tunable diode laser absorption measurements of tropospheric carbon monoxide. *J. Geophys. Res.: Atmos.* **2000**, *105*, 24251−24261.
(42) Pollack, I. B.; Lerner, B. M.; Ryerson, T. B. Evaluation of ultraviolet light-emitting diodes for detection of atmospheric NO_2 by photolysis-chemiluminescence. *J. Atmos. Chem.* **2010**, *65*, 111−125.
(43) Ryerson, T. B.; Huey, L. G.; Knapp, K.; Neuman, J. A.; Parrish, D. D.; Sueper, D. T.; Fehsenfeld, F. C. Design and initial characterization of an inlet for gas-phase NO_y measurements from aircraft. *J. Geophys. Res.: Atmos.* **1999**, *104*, 5483−5492.
(44) Zhao, C.; Wang, Y. Assimilated inversion of NO_x emissions over east Asia using OMI NO2 column measurements. *Geophys. Res. Lett.* **2009**, *36*, L06805.
(45) Zhao, C.; Wang, Y.; Choi, Y.; Zeng, T. Summertime impact of convective transport and lightning NO_x production over North America: modeling dependence on meteorological simulations. *Atmos. Chem. Phys.* **2009**, *9*, 4315−4327.
(46) Zhao, C.; Wang, Y.; Yang, Q.; Fu, R.; Cunnold, D.; Choi, Y. Impact of East Asian summer monsoon on the air quality over China: View from space. *J. Geophys. Res.: Atmos.* **2010**, *115*. DOI: 10.1029/2009jd012745
(47) Zhao, C.; Wang, Y.; Zeng, T. East China plains: A "basin" of ozone pollution. *Environ. Sci. Technol.* **2009**, *43*, 1911−1915.
(48) Liu, Z.; Wang, Y.; Costabile, F.; Amoroso, A.; Zhao, C.; Huey, L. G.; Stickel, R.; Liao, J.; Zhu, T. Evidence of aerosols as a media for rapid daytime HONO production over China. *Environ. Sci. Technol.* **2014**, *48*, 14386−14391.
(49) Gu, D.; Wang, Y.; Smeltzer, C.; Boersma, K. F. Anthropogenic emissions of NO_x over China: Reconciling the difference of inverse modeling results using GOME-2 and OMI measurements. *J. Geophys. Res.: Atmos.* **2014**, *119*, 7732−7740.
(50) Gu, D.; Wang, Y.; Smeltzer, C.; Liu, Z. Reduction in NO x emission trends over China: Regional and seasonal variations. *Environ. Sci. Technol.* **2013**, *47*, 12912−12919.
(51) Gu, D.; Wang, Y.; Yin, R.; Zhang, Y.; Smeltzer, C. Inverse modelling of NO x emissions over eastern China: uncertainties due to chemical non-linearity. *Atmos. Meas. Tech.* **2016**, *9*, 5193−5201.
(52) Zhang, Y.; Wang, Y.; Chen, G.; Smeltzer, C.; Crawford, J.; Olson, J.; Szykman, J.; Weinheimer, A. J.; Knapp, D. J.; Montzka, D. D.; Wisthaler, A.; Mikoviny, T.; Fried, A.; Diskin, G. Large vertical gradient of reactive nitrogen oxides in the boundary layer: Modeling analysis of DISCOVER-AQ 2011 observations. *J. Geophys. Res.: Atmos.* **2016**, *121*, 1922−1934.
(53) Li, J.; Wang, Y. Inferring the anthropogenic NOx emission trend over the United States during 2003-2017 from satellite observations: was there a flattening of the emission trend after the Great Recession? *Atmos. Chem. Phys.* **2019**, *19*, 15339−15352.
(54) Bey, I.; Jacob, D. J.; Yantosca, R. M.; Logan, J. A.; Field, B. D.; Fiore, A. M.; Li, Q.; Liu, H. Y.; Mickley, L. J.; Schultz, M. G. Global

modeling of tropospheric chemistry with assimilated meteorology: Model description and evaluation. *J. Geophys. Res.: Atmos.* **2001**, *106*, 23073−23095.
(55) Henderson, B. H.; Akhtar, F.; Pye, H. O. T.; Napelenok, S. L.; Hutzell, W. T. A database and tool for boundary conditions for regional air quality modeling: description and evaluation. *Geosci. Model Dev.* **2014**, *7*, 339−360.
(56) *Climate Forecast System Reanalysis Products*; Environmental Modeling Center: College Park, MD, 2019; http://cfs.ncep.noaa.gov/cfsr.
(57) Canty, T. P.; Hembeck, L.; Vinciguerra, T. P.; Anderson, D. C.; Goldberg, D. L.; Carpenter, S. F.; Allen, D. J.; Loughner, C. P.; Salawitch, R. J.; Dickerson, R. R. Ozone and NO_x chemistry in the eastern US: evaluation of CMAQ/CB05 with satellite (OMI) data. *Atmos. Chem. Phys.* **2015**, *15*, 10965−10982.
(58) Travis, K. R.; Jacob, D. J.; Fisher, J. A.; Kim, P. S.; Marais, E. A.; Zhu, L.; Yu, K.; Miller, C. C.; Yantosca, R. M.; Sulprizio, M. P.; Thompson, A. M.; Wennberg, P. O.; Crounse, J. D.; St Clair, J. M.; Cohen, R. C.; Laugher, J. L.; Dibb, J. E.; Hall, S. R.; Ullmann, K.; Wolfe, G. M.; Pollack, I. B.; Peischl, J.; Neuman, J. A.; Zhou, X. NO_x emissions, isoprene oxidation pathways, vertical mixing, and implications for surface ozone in the Southeast United States. *Atmos. Chem. Phys.* **2016**, *2016*, 1−32.
(59) Guenther, A. B.; Jiang, X.; Heald, C. L.; Sakulyanontvittaya, T.; Duhl, T.; Emmons, L. K.; Wang, X. The Model of Emissions of Gases and Aerosols from Nature version 2.1 (MEGAN2. 1): an extended and updated framework for modeling biogenic emissions. *Geosci. Model Dev.* **2012**, *5*, 1471−1492.
(60) Washenfelder, R. A.; Attwood, A. R.; Brock, C. A.; Guo, H.; Xu, L.; Weber, R. J.; Ng, N. L.; Allen, H. M.; Ayres, B. R.; Baumann, K.; Cohen, R. C.; Draper, D. C.; Duffey, K. C.; Edgerton, E.; Fry, J. L.; Hu, W. W.; Jimenez, J. L.; Palm, B. B.; Romer, P.; Stone, E. A.; Wooldridge, P. J.; Brown, S. S. Biomass burning dominates brown carbon absorption in the rural southeastern United States. *Geophys. Res. Lett.* **2015**, *42*, 653−664.
(61) Holland, P. W.; Welsch, R. E. Robust Regression Using Iteratively Reweighted Least-Squares. *Commun. Stat. Theor. Methods* **1977**, *6*, 813−827.
(62) Spiess, A. N.; Neumeyer, N. An evaluation of R^2 as an inadequate measure for nonlinear models in pharmacological and biochemical research: a Monte Carlo approach. *BMC Pharmacol.* **2010**, *10*, 6.
(63) Ruckstuhl, A. *Introduction to Nonlinear Regression*; Zurcher Hochschule fur Angewandte Wissenschaften: Winterthur, Switzerland, 2010.
(64) Cynthia Lin, C.-Y.; Jacob, D. J.; Munger, J. W.; Fiore, A. M. Increasing background ozone in surface air over the United States. *Geophys. Res. Lett.* **2000**, *27*, 3465−3468.
(65) Huang, M.; Carmichael, G. R.; Chai, T.; Pierce, R. B.; Oltmans, S. J.; Jaffe, D. A.; Bowman, K. W.; Kaduwela, A.; Cai, C.; Spak, S. N.; Weinheimer, A. J.; Huey, L. G.; Diskin, G. S. Impacts of transported background pollutants on summertime western US air quality: Model evaluation, sensitivity analysis and data assimilation. *Atmos. Chem. Phys.* **2013**, *13*, 359−391.
(66) Lin, M.; Fiore, A. M.; Horowitz, L. W.; Langford, A. O.; Oltmans, S. J.; Tarasick, D.; Rieder, H. E. Climate variability modulates western US ozone air quality in spring via deep stratospheric intrusions. *Nat. Commun.* **2015**, *6*, 7105.
(67) Dunker, A. M.; Koo, B.; Yarwood, G. Contributions of foreign, domestic and natural emissions to US ozone estimated using the path-integral method in CAMx nested within GEOS-Chem. *Atmos. Chem. Phys.* **2017**, *17*, 12553−12571.
(68) Parrish, D. D.; Young, L. M.; Newman, M. H.; Aikin, K. C.; Ryerson, T. B. Ozone designvalues in Southern California's air basins: Temporal evolution and U.S. back-ground contribution. *J. Geophys. Res.: Atmos.* **2017**, *122*, 11166−11182.
(69) Ninneman, M.; Demerjian, K. L.; Schwab, J. J. Ozone production efficiencies at rural New York state locations: Relationship to oxides of nitrogen concentrations. *J. Geophys. Res.: Atmos.* **2019**, *124*, 2363−2376.
(70) Parrish, D. D.; Ennis, C. A. Estimating background contributions and US anthropogenic enhancements to maximum ozone concentrations in the northern US. *Atmos. Chem. Phys.* **2019**, *19*, 12587−12605.

https://doi.org/10.1021/acs.est.1c03035
Environ. Sci. Technol. 2021, 55, 12852−12861